GPR Antenna localization based on A-Scans

Evangelos Skartados[1] Andreas Kargakos[1] Efthimios Tsiogas[1] Ioannis Kostavelis[1]
Dimitrios Giakoumis[1] and Dimitrios Tzovaras[1]

***Abstract*—Automated subsurface mapping with data obtained from Ground Penetrating Radar (GPR) is essential for the construction services. So far, significant progress has been achieved in this domain by integrating such sensors with robotic platforms allowing large scale autonomous subsurface mapping. The paper at hand tackles the challenging issue of self-localization of a GPR antenna in a known subsurface map by utilizing solely GPR measurements. This is achieved by isolating spatiotemporal salient regions on consecutive GPR traces. These regions are represented by utilizing the coefficients of the Discrete Wavelet Transform (DWT) decomposition. Matched representations indicate meaningful tracked regions on the GPR traces that correspond to a fixed time window of data recording. Tracked regions are encoded in the form a vector that is treated as an observation within a particle filtering framework and is further processed to estimate the GPR sensor pose, given (i) a known subsurface map (ii) a simulated GPR model and (iii) priors in the GPR motion model. The GPR antenna self-localization approach has been assessed with real data and exhibited promising results, proving the ability of the proposed method to perform subsurface localization, exploiting only GPR sensor measurements.**

I. Introduction

Recently, significant research endeavors have been applied in the domain of automated subsurface modeling, boosting the technological achievements in the multidisciplinary areas of GPR scanning machinery [1], the GPR signal processing for the detection of buried utilities [2], [3] and the automated large scale subsurface mapping [4], contributing positively to the assessment of underground utilities in urban environments, the subsurface evaluation of energy and mineral production operations, and search and rescue applications at disaster sites.

Subsurface mapping with GPR sensors produces essential representations of the shallow surface providing topological information of the existing infrastructures (e.g. buried pipes), which can be utilized by humans or subsurface operating mechatronic devices, in the form of a metric map. Authors in [4] utilized a GPR antenna towed by a rover to create a coupled surface/subsurface map by associating robot visual odometry with GPR measurements. Similarly, authors in [5] created a three-dimensional, photorealistic surface model coupled with a ribbon of GPR data, and a two-dimensional GPR radargram with the surface topography plotted on top of it. An important limitation of these methods is that they require the existence of the same surface sensing equipment (i.e. vision sensors, GPS, etc.) in order to localize another GPR antenna that operates in the same area, since the subsurface map is amalgamated with the surface one and, thus, subsurface localization derives indirectly. This could benefit applications involving robotic subsurface technologies or applications where robots with GPR antennas operate in environments (e.g. mines) with limited visual sensors and absence of GPS signal.

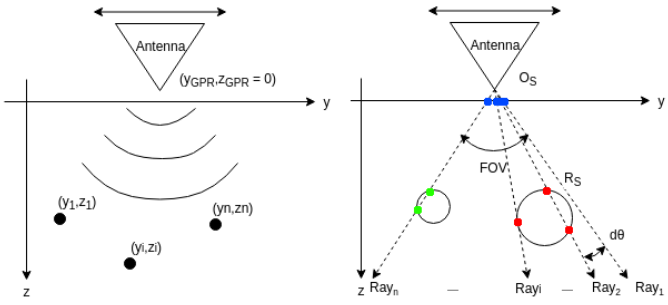

Fig. 1. Models of the real (left) and simulated (right) GPR scanning procedure.

The closest solution to this problem is the work described in [6]. The authors developed a dedicated Localization GPR antenna (LGPR), which has been used in a priori-map-based vehicle localization method, designed to complement existing approaches with a low sensitivity to failure modes of LIDAR, camera, and GPS/INS sensors, due to its low-frequency RF energy. However, in this method the authors assumed as a prior map the aggregated GPR measurements, rather than classical metric maps and performed the localization based on single correlations between the past and current raw GPR measurements, exploiting also Particle Swarm Optimization (PSO), as an optimization technique for fast convergence and search space reduction. Contrary to this approach, our method proposes a GPR sensor localization in a metric subsurface map by exploiting only the GPR measurements -on which signal processing is applied- to create comparative to the metric map representations, allowing the pose estimation of the antenna in the map, without the need of the same perception equipment used during the initial mapping step. Moreover, the proposed method relies on the symbolic representation of the GPR measurements instead of the raw ones, utilizing signal processing by means of the DWT decomposition to form the salient regions representations. Most known methods used for spatial representations of the inspected underground, either deal with it as a typical vision detection problem, an image focusing or a seismic migration problem. They are all applied on B-scans and utilize the hyperbolic pattern that reflections from a certain underground utility are expected to shape on the

[1] All authors are with the Centre for Research and Technology Hellas - Information Technologies Institute (CERTH/ITI), 6^{th} Km Charilaou-Thermi Road, Thessaloniki, Greece, 57001
eskartad@iti.gr

978-9-0827-9703-9/19/$31.00 ©2019 IEEE

stacked A-scans[1] [7]–[10]. Contrary to this, in our method, we process each new trace on-the-fly and infer reflector locations without any reference to long term past or future traces. From another point of view, GPR signal is in general noisy and requires pre-processing steps such as denoising, compression, etc. The DWT is a powerful tool applied in such signal processing domains proved suitable for the frequency analysis of non-stationary signals, such as GPR signals. Successful application of DWT for filtering and denoising purposes of GPR data has been reported in [11], [12], while the authors of [13] applied wavelet analysis so as to perform GPR data classification.

II. GPR Data Processing

A. The model of a real GPR antenna

The first step of our method comprises the modelling of the GPR profile construction process, to be later used in the localization procedure. Planar antenna motion is assumed ($z = 0$), defined by the Z-axis and the axis of GPR movement (see Fig. 1). Along the scanning direction, an electromagnetic stimulating pulse (usually a Ricker wavelet [14]) is transmitted. The voltage magnitude induced at the receiver is sampled over a specific time window. The recorded signal is the result of reflections caused by alterations on the electromagnetic properties of the inspected space and constitutes an A-scan. Such alterations signify the existence of an underground utility, underground clutter or even change on the type of soil. Concatenated A-scans at consecutive sampling positions form a B-scan. Let $p[t]$ denote the stimulating pulse, the received trace $y[t]$ at a specific position is then modeled by $y[t] = \sum_{i=1}^{N} p[t - t_i]$, where N corresponds to the number of point reflectors lying on the YZ plane and t_i corresponds to the total round trip delay between the transmitter and the i^{th} reflector. Hence, the received trace is derived as an overlay of multiple distinct time-shifted replications of the initial pulse, each one originating from a point reflector. In this work, planar reception is assumed for the signal modeling and all scatterers are approached as independent point reflectors with interactions between them being neglected. Underground soil is considered as a lossless medium with conductivity equal to zero. The equation above still manages to convey the most important aspect of the GPR scanning procedure, i.e. a formulation of the time delay of the received reflections. Furthermore, by applying the $d = (v_m \cdot t)/2$ formula, transformation from temporal to spatial reference is achieved, where v_m is the underground wave propagation velocity and the $1/2$ factor accounts for the 2-way travel of wave:

$$y[t] = \sum_{i=1}^{N} p[t - \frac{2 \cdot \sqrt{z_i^2 + (y_i - y_{GPR})^2)}}{v_m}]$$

where $(y_{GPR}, 0)$ are the coordinates of the GPR position and (y_i, z_i) are the coordinates of the i^{th} point reflector.

[1]definition of A-Scan and B-Scan terms are provided in Sect. II-A

B. A-scan Segmentation

As shown on Sec. II-A a single GPR trace is a composition of time-shifted instances of the initial excitatory pulse. This pulse closely resembles to a Ricker wavelet, which is also referred to as Mexican hat wavelet, a name indicative of its waveform, that is centered around a positive peak value. Reflection pulses appearing in an Ascan are expected to have similar waveform. Therefore, positive peak values along the recorded Ascan are indicators of the appearance of reflections of the original pulse. Peak values of the recorded $y[t]$ trace are identified by transforming the $y[t]$ recorded signal into the frequency domain. Fast Fourier Transform is utilized and $j \cdot \omega \cdot Y[\omega]$ and $-\omega^2 \cdot Y[\omega]$ formulas are applied to calculate first and second derivatives. Finally, first and second derivative checks and a sign check are applied to locate local maxima positive values. It should be noted that most of these values correspond to artifacts of the scanning procedure, underground clutter, etc. and only few of them reflect the existence of actual underground utilities.

For each peak a pulse of a predefined length, centered around it, is extracted. The length of the extracted pulses is defined in accordance to the central frequency F_s of the GPR scanning device. Frequencies of reflections are expected to fall symmetrically within a band centered around the central frequency. A rule of thumb is to consider the width of the band equal to $1.5 \cdot F_s$, specifically $[0.25 \cdot F_s, 1.75 \cdot F_s]$. The low frequency of the band defines the largest expected duration of a single reflection pulse in time, which is used to set the predefined length of the extracted segments.

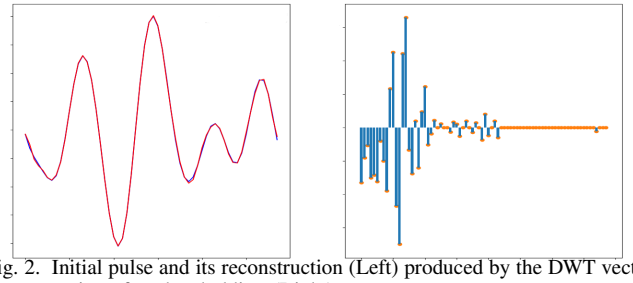

Fig. 2. Initial pulse and its reconstruction (Left) produced by the DWT vector representation after thresholding (Right).

C. Salient Region Description, Matching and Tracking

Instead of forming specific 2D signatures (hyperbolas) over multiple traces, in our proposed method much more relaxed conditions are imposed on the segmented trace regions: (i) the pulses of the current trace should appear consistently in the past few recorded traces and (ii) their amplitudes should be above a certain threshold. The former constitutes a consistency check that forces the generation of a reliable descriptor of the waveform of the extracted pulses that will allow matching among consecutive traces. Discrete Wavelet Transform (DWT) decomposition provides a perfectly invertible multi-resolutional representation of a $1D$ signal that captures information both for the frequency and the time domain. Therefore, DWT is a powerful tool for extracting descriptions of non-stationary signals like the GPR signals that exhibit slow tempo-

ral variations in low frequency and abrupt temporal changes in high frequency. In one level of the DWT the entry signal $y[n]$ (Ascan) is convolved with a high pass filter $h[n]$ and a low pass filter $g[n]$ and is in both cases subsequently down-sampled by two, producing the detail and the approximation coefficients respectively. On a multilevel DWT, approximation coefficients are provided to the next level and the same procedure is repeated. The maximum number of levels the above procedure can be repeated is determined by the length of the original signal and the number of coefficients of the applied filters. From one level to the next one, due to the filtering and the subsampling, the frequency band is reduced to half and at the same time the frequency resolution is doubled. The high-pass filters $h[n]$ comprise the child wavelets of the mother wavelet function and are computed from $\psi_{j,k}[t] = \frac{1}{\sqrt{2^j}}\psi[\frac{t-k2^j}{2^j}]$ where j is the scale parameter accounting for the level of resolution and k is the shift parameter. Low-pass $g[n]$ filters are produced by a function which is referred to as a scaling function. The wavelet family that has been chosen here is Daubechies-6 due to the resemblance of the mother wavelet function to the emitted GPR pulse [15].

Once the decomposition reaches the maximum level, the detail coefficients of all levels along with the approximation coefficients of the maximum level constitute a feature representation of the initial input. Finally, in order to achieve sparsity, only k-most significant coefficients are kept and the rest are set to zero. Fig. 2 illustrates a DWT decomposition example, applied on a pulse of $width = 58$ samples by keeping only the $k = 38$ most significant out of a total of 78 values of the vector and discarding the rest. By applying the inverse procedure on the retained non-zero coefficients, an accurate reconstruction of the original signal is acquired indicating successful sparse representation.

The above procedure is repeated for all extracted pulses. Euclidean distances between feature vectors of pulses from consecutive traces are calculated. Matching is achieved when the distance between a pulse extracted from the current trace and any pulse from the previous trace is below a certain threshold. The matching procedure enables the tracking of the appearance of pulses over time and allows positive identification of a region as a salient one that appears in the last N traces, where $N = 5$ in our particular case.

Furthermore, last $N = 5$ processed samples are used to calculate a moving mean energy of a GPR trace, that is utilized as a threshold on the amplitude of all current candidate pulses: Each reflection pulse is requested to have an amplitude larger than the moving average of values recorded at its time of occurrence. The rationale behind this relies on the assumptions that (i) the amplitude of a pulse originating from a reflector at a considered distance is significantly larger than typical values received when space at that distance is free and (ii) at each considered depth, the underground space is most probably free, biasing moving average towards an estimation of the energy corresponding to free space.

Sufficiently consistent and strong reflection pulses, extracted as described in current section, constitute the salient regions. These regions are described as vectors of distances of the most prominent objects in the subsurface, that are subsequently used as the real observations from the GPR antenna for its localization.

III. Localization based on GPR salient regions

A. Simulated GPR antenna model and ray casting

In our approach, where we introduce a GPR-based particle filtering localization framework, the simulation of the GPR scanning procedure is needed, which in turn requires a world representation. To this end, a representation of the real world needs to be defined. The production of synthetic GPR traces dictates the utilization of a 3D occupancy grid map M, which in our case is a prior generated subsurface map represented as Octomap. The adopted structure is a fine-grained grid over the continuous space of locations where the real world is represented by binary variables indicating the presence of an obstacle at the respective location. The 3D occupancy grid also enables automatic subsurface map generation from past scanning sessions as performed in [4]. During the simulation phase, distance measurements between the GPR model and the obstacles in the map are acquired, by utilizing the volumetric ray casting technique (Fig 1). A geometric ray is generated and traced from an origin point O_S towards the ray's direction. A small variation to the typical ray casting is that all obstacles that lay on the same path of the ray at a distance from the origin O_S smaller than a threshold R_S are retrieved and their corresponding distances are reported. Thus, values in the ray casting are considered only obstacles in the map M, when the cell's assigned probability is higher than a $P_{obstacle}$ threshold.

Having defined the world model and the penetrating ray casting approach, synthetic GPR trace generation is feasible. A 2D slice of the 3D occupancy grip is considered to resemble the model applied on real GPR data acquisition (see Sect. II-A). Given the simulated sensor's pose, a set of geometric rays is generated with common origin O_S. The sample step $d\theta$ is in the interval $[\theta_{min}, \theta_{max}]$ where $\theta_{min} = -FOV/2$ and $\theta_{max} = FOV/2$, where for each angle a new ray with the corresponding direction is produced. The proposed volumetric ray casting method is applied for all emitted rays. The amount of intersected cells corresponding to obstacles depends on the resolution M_{RES} of the utilized 3D grid map and the sampling step $d\theta$ of the set of rays. Finally, 2D intersected cells are clustered together based on their distances from the O_S origin with each cluster represented by the member with the minimum distance.

B. Particle filtering model

A particle filter localization, also known as Monte Carlo localization (MCL), approach has been implemented herein to track a moving antenna's position utilizing the 3D occupancy grid map that contains landmarks of a real underground environment, the real observations and synthetic GPR measurements. The map along with the GPR antenna's measurement model are given as input to the particle filter in order to infer an accurate estimation of the system state (antenna - world).

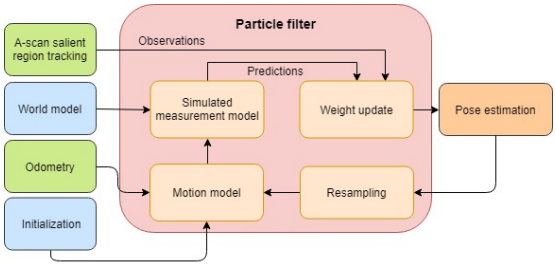

Fig. 3. Particle filter architectural diagram.

The filter's pipeline is illustrated in Fig. 3.

Motion / measurement model: The GPR antenna travels on the YZ-plane with a linear speed (V_y, V_z) that is measured from inertial sensors mounted on its body. At time t, $Observations_t$ correspond to the time of occurrence of tracked salient regions on real GPR measurements, transformed into ranges, while $predictions_t$ is the set of ranges that correspond to a single particle's predicted GPR measurements, according to the simulated model described in Sec. III-A. The filter's pipeline (after one time initialization) is executed at time t only if $Observations_t \neq \emptyset$ and $(V_y, V_z) \neq (0, 0)$.

Initialization: Assuming the antenna's initial position $(P_y, P_z) = (y_0, z_0)$, then N_p particles, corresponding to N_p guesses of the antenna's actual position, are generated using a bivariate Gaussian distribution for variables y and z. The parameters of the Gaussian are $\mu_x = x_0$ and $\mu_y = y_0$ while $\sigma_x = \sigma_y$ depend on the uncertainty level of (P_y, P_z). The cardinality of the particles' set S remains equal to N_p during the localization process. Finally, if p_w is the normalized weight of particle p then $p_w = 1/N_p,\ \forall p \in S$.

Position update: The particles' positions are updated according to the GPR antenna's motion model. A generated Gaussian noise that is sufficiently smaller than the antenna's actual displacement is added to the particles' translation along each axis to incorporate uncertainty in velocity measurements.

Weight update: At time t, the weight of the n^{th} particle is updated taking into account $Observations_t$ and $predictions_t^{[n]}$. A Gaussian distribution is generated for each observation, where μ equals the observed range and σ expresses the estimated error between a real and synthetic measurement. Then, each particle's weight is given by:

$$p_w^{[n]} = \prod_{i=1}^{|Observations_t|} \frac{1}{\sqrt{2\pi\sigma^2}} e^{\frac{-(pred - obs^{[i]})^2}{2\sigma^2}}$$

where $obs^{[i]} \in Observations_t$ is a salient region range and $pred \in predictions_t^{[n]}$ is the predicted range that minimizes $(pred - obs^{[i]})^2$. After the update, the particles' weights are normalized in order to represent a probability distribution, to be used in the resampling step.

Position estimation and Resampling: The antenna's position (P_y, P_z) is estimated by calculating the weighted mean position of all particles in S. Lastly, the resampling procedure takes place. Resampling is performed using a discrete distribution of $i \in [1, N_p]$ to result in the selection of the i^{th} particle, with probability equal to its weight $p_w^{[i]}$. Finally, we set $p_w = 1/N_p, \forall p \in S'$, $|S'| \equiv N_p$ where S' is the resulting particle set.

IV. Methodology Assessment

Table I summarizes the implementation details regarding all aforementioned aspects of the complete pipeline. The method has been tested on subsurface data collected at a realistic test field, using a Stream C GPR antenna made by IDS GeoRadar. The layout of the underground environment is depicted on the top image of Fig.4. An indicative B-Scan acquired by the GPR antenna that performed a scan session of the complete area is provided in the middle. The bottom of Fig. 4 exhibits a synthetically generated B-Scan of the simulated environment. The latter has been produced by replicating the exact same path traversed by the original GPR antenna. The tracking results provided on Fig. 5 depict the output of processing applied on real A-Scans. Different colors correspond to tracked clusters and each cluster entails trace regions matched on consecutive A-Scans. The localization method has been tested on the IDS test field on 9 different experiments with various initial positions. Qualitative results of the pose estimation are provided on Fig. 6 for different time steps of the experiment process. Ground truth and estimated poses are depicted with the green and blue arrows respectively. Each red

TABLE I
Definition of Implementation Parameters

GPR Antenna	Simulated GPR	MCL
$F_{sampling} = 7.3GHz$	$R_S = 6.5m$	$N_p = 500$
$F_{Op} = 600MHz$	$FOV = 80^o$	$\sigma_{Init} = 1$
$TimeWindow = 140ns$	$M_{Resolution} = 0.1$	$F_{exec} = 2Hz$
$SamplingStep = 2.2cm$	$d\theta = 0.1^o$	

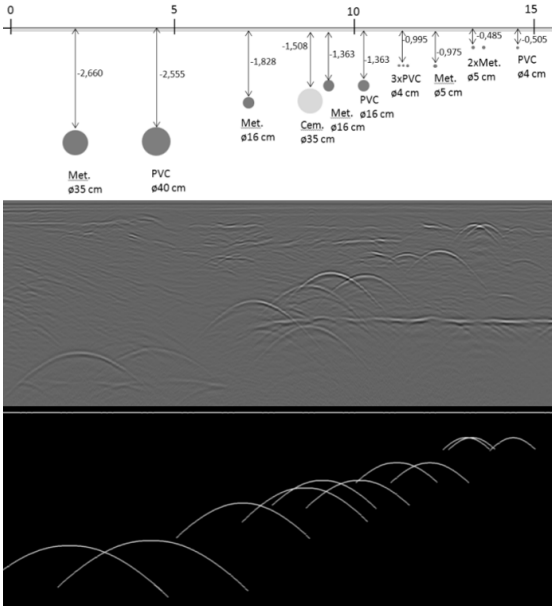

Fig. 4. Ground truth (Top), real B-Scan (Middle) and synthetic B-Scan (Bottom) of the subsurface utilities of IDS test field.

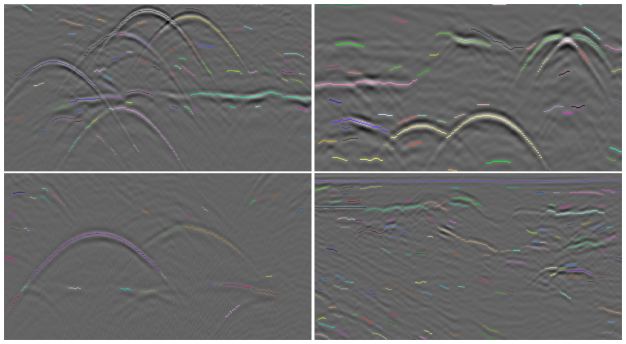

Fig. 5. Examples of salient regions tracking.

arrow represents a pose of a single particle that exists in the current population of the particle cloud. Particles are initially distributed as shown on the first picture and progressively converge to the correct pose. This convergence occurs in only $1.5m$ on average. Moving on to the quantitative results, a mean of root mean square (RMS) error of 0.155 meters is reported over 9 runs. In Fig. 7 the evolution of the RMS error with respect to time for one of the considered sessions is illustrated. Due to the wide variance of the initial distribution, the error is significantly higher in the first iterations but as more observations are processed, the error is reduced to $0.05cm$.

V. Conclusions

In this work, a novel method for GPR antenna localization based on A-scans has been proposed. Through experimental evaluation, it has been proved that the proposed method performs can efficiently localize a GPR antenna in a known subsurface map. GPR A-Scans are expressed in a manner that allows their incorporation into a particle filter algorithm as observations. To achieve this, a simulation model of the GPR sensor has been developed, which along with the subsurface map and the GPR motion model are utilized for localization. Preliminary results on real data yielded sufficiently small localization error. As future extension to the present work, we consider localization of underground GPR antennas along with extension of the current method in high dimensional space.

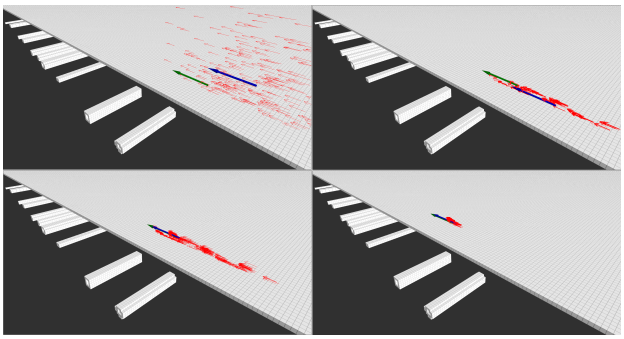

Fig. 6. Experimental setup of GPR scanning session and evaluation of the particle filter.

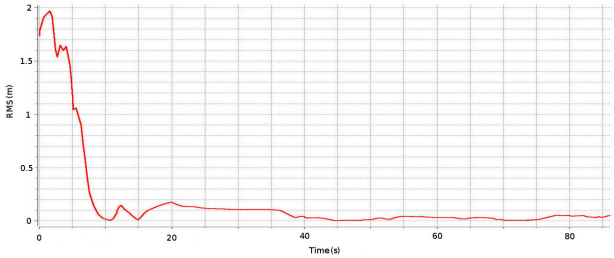

Fig. 7. RMS error (m) with respect to time (s).

Acknowledgement

This work has been supported by the EU Horizon 2020 funded project RoBot for Autonomous unDerGround trenchless opERations, mapping and navigation (BADGER) under the Grant Agreement with no: 731968.

References

[1] X. Feng, M. Sato, Y. Zhang, C. Liu, F. Shi, and Y. Zhao, "Cmp antenna array gpr and signal-to-clutter ratio improvement," *IEEE Geoscience and Remote Sensing Letters*, vol. 6, no. 1, pp. 23–27, 2009.

[2] E. Skartados, I. Kostavelis, D. Giakoumis, A. Simi, G. Manacorda, D. Ioannidis, and D. Tzovaras, "Ground pernetrating radar image processing towards underground utilities detection for robotic applications," *ICCAIRO*, 2018.

[3] A. C. Gurbuz, J. H. McClellan, and W. R. Scott, "Compressive sensing for gpr imaging," in *Conference Record of the Forty-First Asilomar Conference on Signals, Systems and Computers*, IEEE, 2007.

[4] G. Kouros, I. Kotavelis, E. Skartados, D. Giakoumis, D. Tzovaras, A. Simi, and G. Manacorda, "3d underground mapping with a mobile robot and a gpr antenna," in *International Conference on Intelligent Robots and Systems (IROS)*, pp. 3218–3224, IEEE, 2018.

[5] P. Furgale, T. D. Barfoot, N. Ghafoor, K. Williams, and G. Osinski, "Field testing of an integrated surface/subsurface modeling technique for planetary exploration," *The International Journal of Robotics Research*, vol. 29, no. 12, pp. 1529–1549, 2010.

[6] M. Cornick, J. Koechling, B. Stanley, and B. Zhang, "Localizing ground penetrating radar: a step toward robust autonomous ground vehicle localization," *Journal of field robotics*, vol. 33, no. 1, pp. 82–102, 2016.

[7] G. Terrasse, J.-M. Nicolas, E. Trouvé, and É. Drouet, "Automatic localization of gas pipes from gpr imagery," in *EUSIPCO*, pp. 2395–2399, IEEE, 2016.

[8] Q. Hoarau, G. Ginolhac, A. M. Atto, J.-M. Nicolas, and J. P. Ovarlez, "Robust adaptive detection of buried pipes using gpr," in *24th EUSIPCO*, pp. 533–537, IEEE, 2016.

[9] S. Lameri, F. Lombardi, P. Bestagini, M. Lualdi, and S. Tubaro, "Landmine detection from gpr data using convolutional neural networks," in *25th EUSIPCO*, pp. 508–512, IEEE, 2017.

[10] R. Stolt, "Migration by fourier transform," *Geophysics*, vol. 43, no. 1, pp. 23–48, 1978.

[11] S.-H. Ni, Y.-H. Huang, K.-F. Lo, and D.-C. Lin, "Buried pipe detection by ground penetrating radar using the discrete wavelet transform," *Computers and Geotechnics*, vol. 37, no. 4, pp. 440–448, 2010.

[12] J. Baili, S. Lahouar, M. Hergli, A. Amimi, and K. Besbes, "Application of the discrete wavelet transform to denoise gpr signals," in *2nd International Symposium on Communications, Control and Signal Processing, Marrakech, Morocco*, p. 11, 2006.

[13] W. Shao, A. Bouzerdoum, and S. L. Phung, "Sparse representation of gpr traces with application to signal classification," *IEEE transactions on geoscience and remote sensing*, vol. 51, no. 7, pp. 3922–3930, 2013.

[14] G. Terrasse, J.-M. Nicolas, E. Trouvé, and É. Drouet, "Sparse decomposition of the gpr useful signal from hyperbola dictionary," in *EUSIPCO*, pp. 2400–2404, IEEE, 2016.

[15] J. Baili, S. Lahouar, M. Hergli, I. L. Al-Qadi, and K. Besbes, "Gpr signal de-noising by discrete wavelet transform," *Ndt & E International*, vol. 42, no. 8, pp. 696–703, 2009.